Porphyrin Nanoassemblies *via* Surfactant-Assisted Assembly and Single Nanofiber Nanoelectronic Sensors for High-Performance H_2O_2 Vapor Sensing

Peipei Guo,[†,⊥] Guangyao Zhao,[†,⊥] Penglei Chen,[*,†,‡] Bin Lei,[†,‡,⊥] Lang Jiang,[†] Hantang Zhang,[†] Wenping Hu,[*,†,§] and Minghua Liu[*,†]

[†]Beijing National Laboratory for Molecular Science, Institute of Chemistry, Chinese Academy of Sciences, No. 2 Zhongguancun Beiyijie, Beijing 100190, People's Republic of China, [‡]College of Chemistry and Molecular Engineering, Zhengzhou University, 100 Science Road, Zhengzhou Henan 450001, People's Republic of China, and [§]Collaborative Innovation Center of Chemical Science and Engineering (Tianjin) Tianjin 300072, People's Republic of China. [⊥]These authors contributed equally to this work.

ABSTRACT Porphyrins are recognized as important π-conjugated molecules correlating supramolecular chemistry, nanoscience, and advanced materials science. So far, as their supramolecular nanoassemblies are addressed, most efforts focus on the photo- or opto-related subjects. Beyond these traditional subjects, it is strongly desired to develop advanced porphyrin nanoassemblies in some other new topics of paramount importance. By means of a surfactant-assisted assembly, we herein show that porphyrins of different central metal ions, 5,10,15,20-tetra(4-pyridyl)-21*H*,23*H*-porphine (H2TPyP), zinc 5,10,15,20-tetra(4-pyridyl)-21*H*,23*H*-porphine (ZnTPyP), and oxo-[5,10,15,20-tetra(4-pyridyl)porphyrinato]titanium(IV) (TiOTPyP), could be organized to form irregular aggregates, short nanorods, and long yet straight nanofibers, respectively. Remarkably, in terms of an organic ribbon mask technique, we show that such long yet straight TiOTPyP nanofibers could be integrated into single nanofiber-based two-end nanoelectronics. Such simple nanodevices could serve as high-performance sensors of a satisfactory stability, reproducibility, and selectivity for an expeditious detection of vapor-phase H_2O_2. This provides a new alternative for a fast sensing of vapor-phase H_2O_2, which is currently an important issue in the fields of anti-terrorism, industrial healthcare, *etc.* In contrast to the traditional investigations focusing on the photo- or opto-related topics, our work endows porphyrin nanostructures with new opportunities as advanced nanomaterials in terms of portable yet high-performance nanoelectronic sensors, which is an issue of general concern in modern advanced nanomaterials.

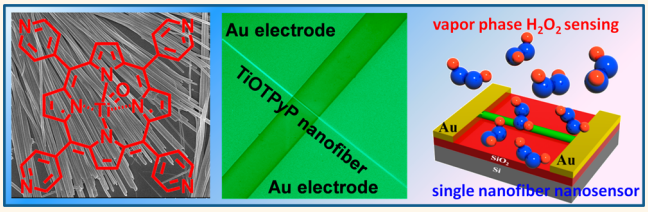

KEYWORDS: supramolecular nanomaterials · nanofibers · nanoelectronic sensors · self-assembly · π-conjugated molecules

One of the most important bridges correlating supramolecular chemistry, nanoscience, and advanced materials science is π-conjugated molecules,[1−8] wherein porphyrins have received particular attention.[1,4,9−31] This is promoted by their well-understood rigid and planar geometric structures, their distinctly featured and readily tailored spectroscopic and photochemical properties, and their well-known multifunctionality and biocompatibility. These issues render their supramolecular nanoarchitectures emerging candidates for the development of advanced supramolecular nanomaterials in numerous fields of paramount importance.[1,4,9−31] So far, as the nanostructured porphyrin supramolecular assemblies are addressed, most efforts focus on their potential applications in photo- or opto-related subjects, including photoelectronics, nonlinear optical devices, photocatalysts, energy conversion, chiroptical systems, mimicking the photosynthetic process occurring in nature systems, *etc.*[9−17,24−27] Considering the distinguished multifunctionality of porphyrin molecules, it is strongly desired to develop advanced porphyrins of potential applications in some other new areas of paramount importance other than the traditional photo- or opto-related subjects.[32−34] This might open up new and varied opportunities for porphyrin-based supramolecular nanomaterials.

To address this important issue, we herein report a surfactant-assisted self-assembly (SAS) of three kinds of porphyrins of different central metal ions, a free-base porphyrin, 5,10,15,20-tetra(4-pyridyl)-21*H*,23*H*-porphine (H2TPyP), and two metalloporphyrins, zinc

* Address correspondence to chenpl@iccas.ac.cn, cpl@zzu.edu.cn, huwp@iccas.ac.cn, liumh@iccas.ac.cn.

Received for review November 25, 2013 and accepted March 23, 2014.

Published online March 24, 2014
10.1021/nn406071f

5,10,15,20-tetra(4-pyridyl)-21*H*,23*H*-porphine (ZnTPyP) and oxo-[5,10,15,20-tetra(4-pyridyl)porphyrinato]titanium(IV) (TiOTPyP), wherein sodium dodecyl benzene sulfonate (SDBS) is used as surfactant (Scheme 1). We find that simply by dropping a chloroform solution of these porphyrins into a SDBS aqueous solution, substantially distinct supramolecular nanostructures, whose morphology depends on the central metal ions, could be assembled. For H2TPyP, irregular nanostructures accompanied by a small amount of 1D nanospecies are formed, while short nanorods are obtained when ZnTPyP is assembled under similar experimental conditions. Interestingly, when the central metal ion is Ti═O, straight yet long nanofibers of *ca.* 30−60 μm come into being. More significantly, by an organic ribbon mask technique, such long yet straight nanofibers of TiOTPyP could be integrated into single nanofiber-based two-end nanoelectronics. Such simple nanodevices could exhibit a fast, reversible, stable, and reproducible response toward vapor-phase H_2O_2, while the irregular nanospecies formed by H2TPyP and the short nanorods formed by ZnTPyP could not.

The significance of our work is three-fold. On one hand, it likely provides new scientific clues on the design of desired porphyrins for the assembly of well-defined advanced supramolecular functional nanomaterials. Considering the abundant diversity of π-conjugated molecules, the obtained scientific information might be extended to other π chromophores other than porphyrins. On the other hand, in terms of single nanofiber nanoelectronic sensors, our work might provide an alternative way for vapor-phase H_2O_2 sensing, which is currently an important issue in anti-terrorism and industrial healthcare issues, *etc.* Moreover, beyond the traditional investigations focusing on the photo- or opto-related areas, our work likely endows porphyrin nanostructures with new opportunities as advanced nanomaterials in terms of portable yet high-performance nanoelectronic sensors, which is an issue of general concern in modern advanced functional nanomaterial science.

RESULTS AND DISCUSSION

First, we investigate the assembly behaviors of H2TPyP and ZnTPyP. To demonstrate the role played by SDBS, we attempted to accomplish the assembly by dropping a chloroform (oil) guest solution of these porphyrins into a host solution of plain water, wherein no SDBS surfactant was dissolved. In these cases, purple aggregates adsorbed on the stirring bar and the wall of the assembly vial, or floating on the surface of the dispersions could be observed after the evaporation of chloroform (Supporting Information Figure S1). As shown in Figure S2, the as-obtained colorless dispersions exhibit only negligible absorptions, while the chloroform solutions of these porphyrins exhibit a distinct Soret band at *ca.* 418 (H2TPyP) and 425 (ZnTPyP) nm. These results indicate that our porphyrins could hardly be

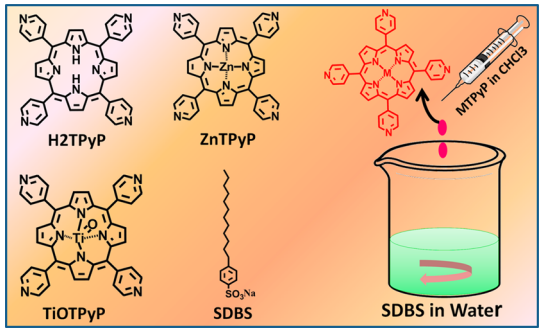

Scheme 1. Molecular structure of H2TPyP, ZnTPyP, TiOTPyP, and SDBS. Right panel: schematic illustration of our SAS protocol.

introduced into plain water phase by chloroform because they are almost water-insoluble, and at the same time, chloroform is unmixable with water. Nevertheless, the aggregates floating on the surface of the dispersions or absorbed on the stirring bar were collected and their SEM images were measured. As shown in Figure S3, irregular structures are observed. These observations imply that our porphyrins could not be assembled to form well-defined supramolecular nanoarchitectures when plain water, wherein no surfactant is dissolved, is employed as host solvent.

In contrast, when an aqueous solution of SDBS was used as host solution, turbid dispersions were obtained immediately after addition of a chloroform solution of these porphyrins. Transparent dispersions with a yellowish (H2TPyP) or greenish (ZnTPyP) color were obtained after the evaporation of chloroform (Figure S4). These observations indicate that, with the assistance of SDBS surfactants, our porphyrins originally dispersed in the oil phase could be introduced into the aqueous phase. As shown in Figure 1A, for the H2TPyP system, the UV−vis spectrum of the as-produced dispersion displays a distinct yet broad Soret band centered at *ca.* 423 nm. Compared to that of the H2TPyP dissolved in chloroform, this band exhibits a red shift of *ca.* 5 nm. This result suggests that our H2TPyP molecules might form various non-specific J-like assemblies in the dispersion.[35−39] The SEM image of the as-produced structures was measured. As shown in Figure 1B, irregular nanostructures, which are approximately similar to those produced using plain water as host solution (Figure S3A), were observed. Besides, a small amount of 1D nanostructures could also be observed occasionally. These observations basically indicate that most of our H2TPyP molecules could not be assembled to form well-defined supramolecular nanoarchitectures with the assistance of SDBS, although it could be introduced into the aqueous phase successfully.

On the other hand, when ZnTPyP molecules are assembled under similar experimental conditions, the situation changes evidently. As shown in Figure 1C, the UV−vis spectrum of the dispersion displays a Soret band at *ca.* 432 nm, which also exhibits a bathochromic

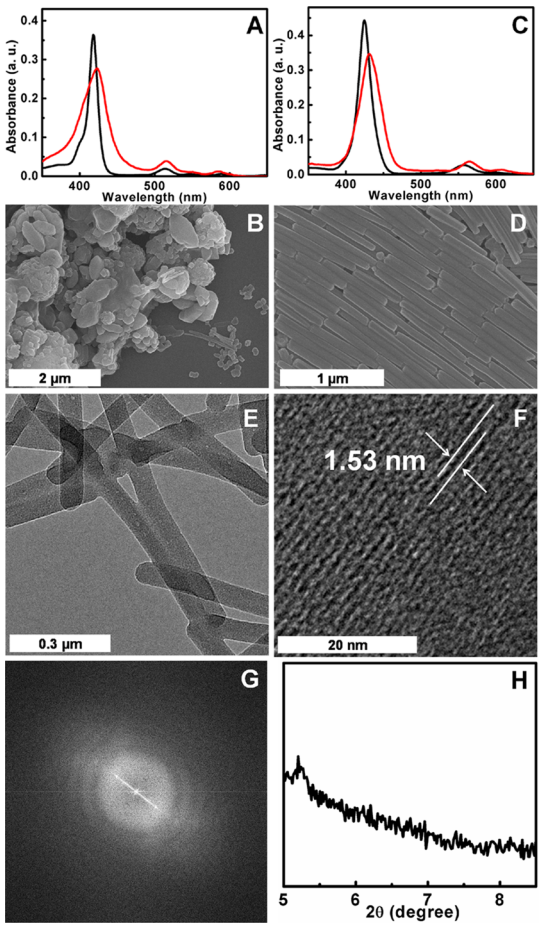

Figure 1. (A) UV−vis spectrum of H2TPyP dissolved in chloroform (black) and that of the corresponding dispersion (red) obtained by our SAS. (B) SEM image of H2TPyP aggregates obtained *via* our SAS. (C) UV−vis spectrum of ZnTPyP dissolved in chloroform (black) and that of the corresponding dispersion (red) obtained by our SAS. (D) SEM, (E) TEM, and (F) HRTEM images of ZnTPyP nanorods. (G) FFT pattern of the corresponding HRTEM shown in panel F. (H) XRD pattern of the ZnTPyP nanorods.

shift compared to that of the monomeric ZnTPyP located at *ca.* 425 nm. However, this band manifests itself with a relatively sharper profile compared to the broad Soret band of the non-specific J-like assemblies of H2TPyP (Figure 1A). These results preliminarily suggest that, different from its free-base counterpart H2TPyP, our ZnTPyP molecules might form well-defined J-like aggregates.[35−39] The SEM and TEM images of the formed ZnTPyP aggregates were investigated. As shown in Figure 1D,E, nanorods with a diameter of *ca.* 80 nm and a length of approximately 300−1200 nm could be observed by SEM and TEM, further confirming the formation of well-defined aggregates. This is different from the irregular nanospecies of ZnTPyP assembled without the assistance of SDBS (Figure S3B). Meanwhile, it is also different from that of H2TPyP obtained with or without the assistance of SDBS (Figures 1B and S3A).

To disclose their internal structural features, the high-resolution transmission electron microscopy (HRTEM), fast Fourier transformation (FFT), and X-ray diffraction (XRD) of these nanorods were investigated. As shown in Figure 1F, it can be seen that lattice fringes, which are aligned along the axis of the nanorod, could be observed distinctly. An interlattice spacing of *ca.* 1.53 nm could be obtained from the HRTEM image or derived by the FFT analysis (Figure 1G). This value is very close to the diagonal of the ZnTPyP square, which is calculated to be *ca.* 1.56 nm. Together with the results of UV−vis spectra (Figure 1C) and SEM image (Figure 1D), these facts indicate that our ZnTPyP nanorods are composed of parallel aligned 1D J-like aggregates of ZnTPyP chromophores. This could be verified by the XRD pattern of the nanorods (Figure 1H), wherein a diffraction peak at $2\theta = 5.3°$, indicating an interlattice distance of *ca.* 1.66 nm, could be observed. This value is nearly similar to the diagonal of the ZnTPyP square and also to interlattice spacing obtained from HRTEM (Figure 1F) and FFT (Figure 1G), confirming that the ZnTPyP units could be organized to form well-defined supramolecular nanoassemblies *via* our SAS.

For SAS, it is necessary that an appropriate intermolecular interaction exists between the surfactant and the investigated molecules,[40−43] wherein the formation of well-defined supramolecular nanoarchitectures is a result of the competition of porphyrin−surfactant interactions and porphyrin−porphyrin interactions.[19,28−31] As evidenced by the irregular nanospecies formed using plain water as host solution (Figure S3), it can be suggested that when porphyrin−SDBS interactions do not participate in the competition, the porphyrin−porphyrin interactions in terms of intermolecular $\pi-\pi$ and hydrophobic interactions,[19,36,38] which predominate the assembly in this case, disfavor the formation of well-defined supramolecular nanoarchitectures. On the other hand, in the case of SAS, the SDBS−porphyrin interactions would compete with the porphyrin−porphyrin interactions. For the H2TPyP SAS system, the SDBS plays a negligible role because, similar to those obtained using plain water as host solution (Figure S3A), most of the formed aggregates in this case manifest themselves as irregular species (Figure 1B), although some 1D nanostructures could also be observed on occasion.

Generally, free-base porphyrins have a nice planarity,[36,38,44−46] favoring the intermolecular porphyrin−porphyrin interactions. Consequently, the SDBS−H2TPyP interactions might be at a disadvantage status in the competition such that the strong H2TPyP−H2TPyP interactions dominate the assembly, facilitating the formation of irregular nanospecies. In contrast, compared to their counterparts of free-base porphyrins, Zn stands out of the porphyrin plane in zinc porphyrins.[44,45] This would lead to some changes in charge distribution and at the same time bring about steric hindrance between ZnTPyP molecules,[45] thus weakening the porphyrin−porphyrin intermolecular interactions.[36,38,46] Accordingly, different from the case of H2TPyP, the role

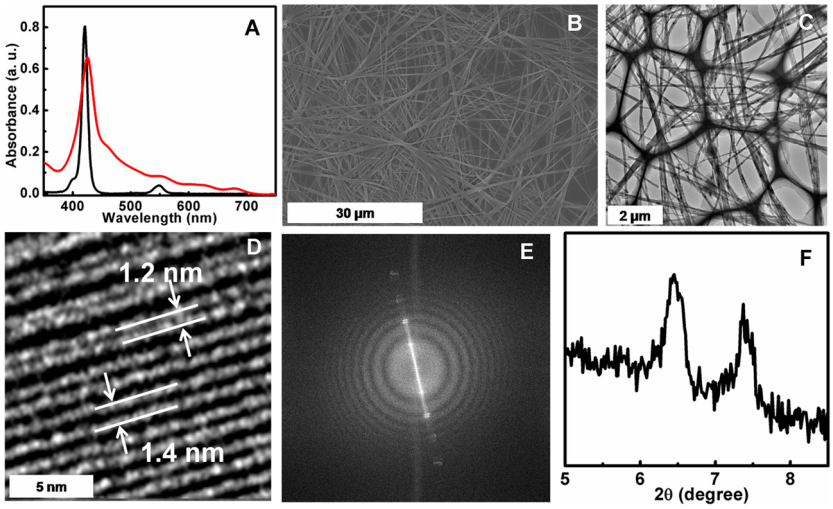

Figure 2. (A) UV−vis spectrum of TiOTPyP dissolved in chloroform (black) and that of the corresponding dispersion (red) obtained by SAS. (B) SEM, (C) TEM, and (D) HRTEM images of TiOTPyP nanofibers. (E) FFT pattern of the corresponding HRTEM shown in panel D. (F) XRD pattern of TiOTPyP nanofibers.

played by the SDBS−ZnTPyP interactions during the SAS of ZnTPyP could not be neglected. The result is that ZnTPyP/surfactant complexes, which are mainly driven by the hydrophobic interactions[19,41−43,47,48] and $\pi-\pi$ interactions[30] between surfactant and ZnTPyP, are formed upon the meeting of ZnTPyP and SDBS in the oil (chloroform)-in-water medium. With the evaporation of chloroform, the ZnTPyP/SDBS complexes disassemble (Figure S5), and the released ZnTPyP molecules begin to self-assemble,[29,30] wherein the directionality of the $\pi-\pi$ interactions induces the formation of 1D nanostructures.[28−30,49,50]

It thus could be seen that, although only slight difference exists between H2TPyP and ZnTPyP molecules, substantially different supramolecular nanoarchitectures could be produced *via* our SAS. The steric hindrance and the changes in the charge distribution, which are induced by the existence of zinc cation in the cavity of ZnTPyP, might play a critical role. As known, TiOTPyP is another important metalloporphyrin, wherein there is an oxygen ligand that axially coordinates to the central titanium cation (Scheme 1). This would also bring about some changes in the charge distribution and steric hindrance between TiOTPyP molecules when they are assembled. To verify the above-mentioned proposals, the TiOTPyP molecules were also assembled *via* our SAS under similar experimental conditions.

As shown in Figure 2A, the TiOTPyP molecules dissolved in chloroform display a sharp Soret band at *ca.* 421 nm. For the assemblies obtained *via* our SAS, a red-shifted yet sharp Soret band at *ca.* 426 nm could be observed. This indicates that, similar to its counterpart ZnTPyP, our TiOTPyP might also form well-defined J-like aggregates. This preliminarily verifies the above proposal that the steric hindrance and the changes in the charge distribution caused by the central metal ions likely play an important role for the assembly of our porphyrins. Besides, it is noted that a shoulder Soret band around 460 nm could also be observed. This observation indicates that, in the as-assembled TiOTPyP nanostructures, there might be two kinds of J-like aggregates, which are different from each other in their molecular stacking style.[51] As indicated by the SEM image of the samples shown in Figure 2B, long yet straight 1D nanostructures with a diameter of *ca.* 70−200 nm and a length of *ca.* 30−60 μm could be observed. These structural features could be further confirmed by the TEM investigation, as shown in Figure 2C.

To reveal the internal structure of these 1D nanofibers, their HRTEM, FFT, and XRD were measured. As shown in Figure 2D, distinct lattice fringes could be observed from the HRTEM image, wherein the parallel nanostripes were aligned along the axis of the nanofibers. Interestingly, besides an interlattice distance of *ca.* 1.4 nm, which is close to the diagonal of the TiOTPyP square, another interlattice spacing of *ca.* 1.2 nm, which is close to the side length of the TiOTPyP square, could also be deduced from the HRTEM (Figure 2D) and FFT (Figure 2E) of the nanofibers. This result is different from that of the ZnTPyP nanorods, wherein only one interlattice spacing could be obtained (Figure 1F−H). Accompanied by the facts observed from UV−vis spectra shown in Figure 2A, this result further suggests that TiOTPyP molecules mainly form two kinds of J-like aggregates in the nanofibers, in which the TiOTPyP chromophores stack with or without an interplanar staggering angle.

Different from ZnTPyP, there is an axial oxygen ligand anchored on the macrocycle of TiOTPyP, endowing it with a pyramidal geometry. Consequently, there might exist various aggregation styles in the assemblies, namely, face-to-face, back-to-back, and

face-to-back configurations.[46] We tentatively suggest that these multiple packing configurations might be related to the observations that two kinds of J-like aggregates (namely, with or without an interplanar staggering angle) are formed in the formulated nanostructures. We, however, have to stress that a detailed understanding concerning this issue is still unclear at the present stage. Nevertheless, two diffraction peaks at 2θ = 6.44 and 7.44°, indicating an interlattice distance of 1.37 and 1.19 nm, respectively, could be observed from the XRD pattern of the nanofibers, as shown in Figure 2F. These values are in good agreement with the interlattice spacing obtained by HRTEM (Figure 2D) and FFT (Figure 2E), further verifying the existence two kinds of J-like aggregates in the TiOTPyP nanofibers. Together with the results of H2TPyP and ZnTPyP, the present facts imply that the steric hindrance and the changes in the charge distribution induced by the central metal ions might contribute much to the different supramolecular nanoarchitectures formed by our porphyrins.

Currently, nanoelectronic sensors based on an individual 1D nanoarchitecture have been attracting widespread interest[52−56] because the high aspect ratio of the 1D nanostructures favors a rapid capture, diffusion, and release of the detected molecules, facilitating the formulation of miniature yet high-performance nanosensors of expeditious response/recovery. Practically, for nanoelectronics of a single 1D nanostructure, it is necessary that the addressed nanoarchitectures should be straight yet long enough for the integration of an individual nanospecies into nanoelectronics by laboratory fabrication protocols.[52−58] As shown in Figure 2B,C, by means of our SAS, TiOTPyP could be assembled into straight nanofibers with a length of *ca.* 30−60 μm. By taking advantage of this structural feature, an individual TiOTPyP nanofiber was built into two-end nanoelectronics *via* an organic ribbon mask technique using Au as the electrodes,[57] as illustrated in Figure 3A. Experimentally, we found that the irregular aggregates formed by H2TPyP and the short nanorods formed by ZnTPyP could not be integrated in such simple two-end nanodevices, owing to their irregularity and short length, respectively.

As a preliminary example for a proof-of-concept application of our single nanofiber devices, their electrical characteristics in terms of the responses toward H_2O_2 vapor were investigated at 25 °C (Figure 3B). As shown in Figure S6A, when the device is dosed with a flow of 0.25 ppm H_2O_2 vapor, its electrical current displays a significant increase immediately within *ca.* 2 s. In contrast, when the flow of the H_2O_2 vapor is switched off and that of N_2 gas switched on, the electrical current recovers to its original value instantly within *ca.* 10 s. As shown in Figure 4A, the sensor response of our devices, which is defined as the percent current alterations of the devices, % current

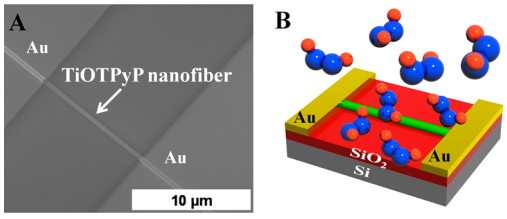

Figure 3. (A) SEM image of the prototype two-end nanodevice constructed *via* an organic ribbon mask method. (B) Schematic illustration of single TiOTPyP nanofiber nanoelectronic sensors for vapor-phase H_2O_2 sensing. The drawings are not to scale.

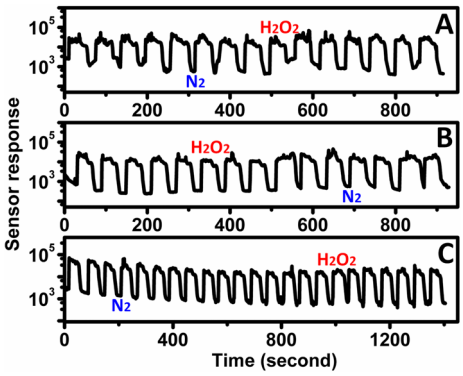

Figure 4. Sensor response of our single nanofiber devices toward a flow of H_2O_2 vapor of *ca.* 0.25 ppm at 25 °C. (A) Device 1. (B) Device 2. (C) Device 3.

alternations = $|[(I_{H_2O_2} - I_{N_2})/I_{N_2}]| \times 100$ ($I_{H_2O_2}$ and I_{N_2} are the electrical current of the device under H_2O_2 vapor and N_2 atmospheres, respectively),[59] is estimated to be as high as *ca.* 2.1 × 10^4. On one hand, such quick and reversible electrical performances could be operated repeatedly and reproducibly many times during each response/recovery cycle. On the other hand, as shown in Figures 4 and S6, three different devices display almost similar sensor response (around 2.1 × 10^4) and electrical performances under similar experimental conditions. These results indicate a satisfactory reproducibility and stability of our nanoelectronics. As shown in Figures 5A,B and S7, when our nanodevices are dosed with a flow of H_2O_2 vapor of *ca.* 1.25 and 2.5 ppm, approximately similar expeditious and reversible electrical performances could be observed. Compared to that of *ca.* 2.1 × 10^4 obtained by dosing with 0.25 ppm H_2O_2 vapor, the sensor response in these cases increases to as high as *ca.* 3.9 × 10^4 and 7.1 × 10^4, respectively. As plotted in Figure 5C, there is a linear correlation between sensor response and the concentration of the dosed H_2O_2 vapor, indicating the bright future of our single nanofiber nanoelectronics toward H_2O_2 vapor sensing.

As known, vapor-phase concentration of H_2O_2 is generally sensitive to ambient temperature.[60] The effects of temperature on sensor performances were also investigated. As shown in Figure 6A, a sensor response of *ca.* 5.3 × 10^3 is obtained when a flow of H_2O_2 vapor, which is generated by a H_2O_2 aqueous

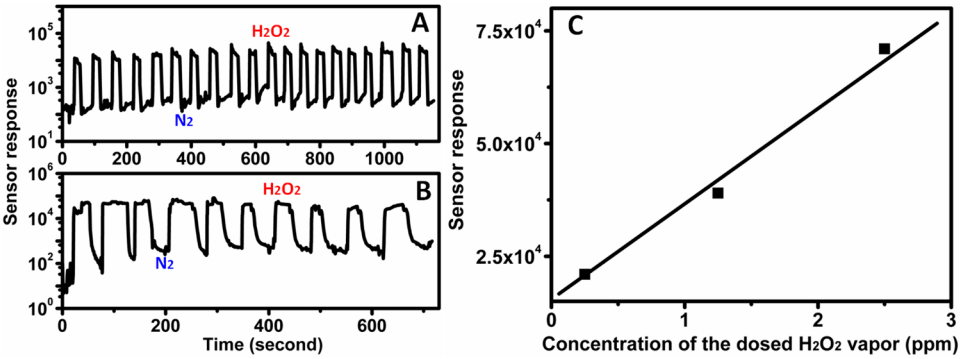

Figure 5. Sensor response of our single nanofiber devices toward a flow of H_2O_2 vapor of *ca.* 1.25 (A) and 2.5 (B) ppm at 25 °C. (C) Correlation between sensor response and the concentration of the dosed H_2O_2 vapor.

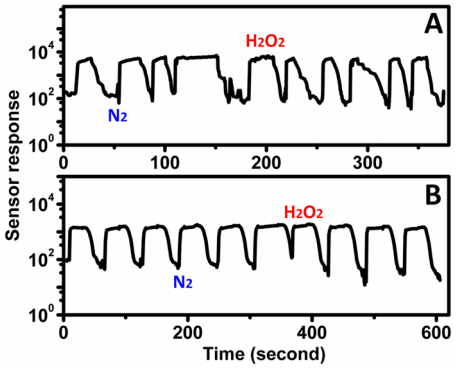

Figure 6. Sensor response of our nanofiber nanodevices toward a flow of H_2O_2 vapor, which is generated by a H_2O_2 aqueous solution of *ca.* 0.09 wt % at 0 (A) and 35 (B) °C.

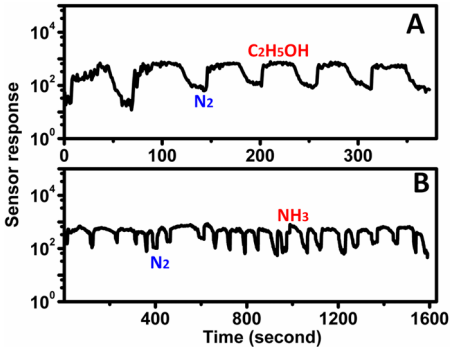

Figure 7. Sensor response of our single nanofiber devices toward a flow of C_2H_5OH (A) and NH_3 (B) gases of *ca.* 0.25 ppm at 25 °C.

solution of 0.09 wt % at 0 °C (in this case, the vapor-phase concentration of H_2O_2 is *ca.* 0.035 ppm),[60] is dosed. In contrast, as shown in Figure 4, the sensor response increases to *ca.* 2.1×10^4 when a flow of H_2O_2 vapor, which is generated by a H_2O_2 aqueous solution of 0.09 wt % at 25 °C (in this case, the vapor-phase concentration of H_2O_2 is *ca.* 0.25 ppm),[60] is detected. This result confirms that the vapor-phase H_2O_2 concentration could influence sensor performance. On the other hand, as shown in Figure 6B, the sensor response decreases to *ca.* 1.3×10^3 when a flow of H_2O_2 vapor, which is generated by a H_2O_2 aqueous solution of 0.09 wt % at 35 °C (in this case, the vapor-phase concentration of H_2O_2 is *ca.* 0.50 ppm),[60] was dosed. These observations suggest that, besides the vapor-phase concentration, the performance of our devices might also be affected by the temperature of the H_2O_2 vapor itself. Nevertheless, these results indicate that our single nanofiber-based nanosensors are workable in a temperature range of 0−35 °C, which could meet the requirements of routine analyses. Besides H_2O_2, C_2H_5OH and NH_3 gases were also detected using our nanodevices. As shown in Figure 7, compared to that of *ca.* 2.1×10^4 obtained from the sensing of 0.25 ppm H_2O_2 vapor at 25 °C (Figure 4), the sensor response decreases to as low as *ca.* 7.3×10^2 and 4.7×10^2, respectively, when 0.25 ppm C_2H_5OH and NH_3 gases is dosed. These results demonstrate that our nanofiber devices have an acceptable selectivity toward H_2O_2 vapor.

As known, an expeditious sensing of H_2O_2 species has currently been recognized as one of the most important issues in various fields of paramount importance, such as photochemistry, food chemistry, biochemistry, healthcare, and counterterrorism, *etc.*[61−64] However, most of the sensing protocols, including electrochemical sensing, chemiluminescence, fluorescence, spectrophotometry *etc.*, generally suffer from either detection in solution only or the requirement of bulky yet expensive apparatus.[61−64] To address these challenges, electronic-based gas sensors in terms of a thin-film geometry have been recently developed.[65,66] In those cases, the response/recovery time of the thin-film devices is generally several minutes, which is much larger than that of our present single nanofiber-based nanoelectronics. We also fabricated our TiOTPyP-based electronic devices using thin-film geometry and investigated their responses to vapor-phase H_2O_2. As shown in Figure S8, upon being dosed with a H_2O_2 vapor of *ca.* 2.5 ppm, our thin-film electronics also display reversible responses during the H_2O_2 vapor/N_2 gas switched on/off procedure, wherein a sensor response of *ca.* 5.2×10^3 is obtained. This value is distinctly smaller than the *ca.* 7.1×10^4 of our single nanofiber-based

devices measured under similar experimental conditions (Figure 5B). The response and recovery time of our thin-film devices is *ca.* 9 and 60 s, respectively. In contrast, the corresponding data of our nanofiber-based devices are *ca.* 2 and 25 s, respectively. These data are smaller than those of our thin-film-based sensors, indicating that, compared to the devices of thin-film geometry, our single nanofiber-based electronics could work as high-performance sensors of expeditious response/recovery for H_2O_2 detection. This is due to the fact that, compared to the thin films, the high aspect ratio of the 1D nanostructures favors a rapid capture, diffusion, and release of the detected molecules.[61] As a matter of fact, electronic gas nanosensors in terms of nanofiber geometry have recently been developed for O_2 sensing.[67] Different from our present cases, the devices therein were not composed of a single 1D nanostructure but *ca.* 3×10^4 nanorods. In that case, a response/recovery time of several hours was generally required for the operation of the devices. Our single nanofiber-based two-end electronic nanosensor might be a good example of proof-of-concept applications for an expeditious and facile detection of H_2O_2 vapor.

CONCLUSION

In summary, we report that porphyrins of different central metal ions could be assembled to form nanostructured assemblies of distinct architectures *via* a SAS. It is disclosed that the free-base porphyrin H2TPyP could only be assembled to form irregular nanospecies, while its counterpart of metalloporphyrin ZnTPyP could be assembled to form short nanorods. Interestingly, long yet straight 1D nanofibers could be obtained when the TiOTPyP molecules are assembled in the same way. Our results suggest that the steric hindrance and changes in the charge distribution induced by the central metal ions might contribute much for the interesting assembly behaviors of our porphyrins. We envision that, beyond the porphyrins, the scientific information presented herein might be extended to other desired π-conjugated systems. Remarkably, we show that an individual TiOTPyP nanofiber could be integrated into two-end nanoelectronics, while the nanostructures formed by H2TPyP and ZnTPyP could not. More significantly, we demonstrate that such simple two-end nanoelectronics could work as high-performance sensors of satisfactory reproducibility, stability, and selectivity for an expeditious detection of vapor-phase H_2O_2. At the present stage, it should be pointed out that it is difficult to detect liquid-phase H_2O_2 using our nanodevices because an electrolysis of water occurs when a bias voltage is applied on our electronics. Further study on this important issue is underway in our lab.

METHODS

Chemicals and Materials. 5,10,15,20-Tetra(4-pyridyl)-21*H*,23*H*-porphine (H2TPyP, Aldrich, 97%), zinc 5,10,15,20-tetra(4-pyridyl)-21*H*,23*H*-porphine (ZnTPyP, Aldrich, 90%), oxo-[5,10,15,20-tetra-(4-pyridyl)porphyrinato]titanium(IV) (TiOTPyP, TCI, >90.0%), sodium dodecyl benzene sulfonate (SDBS, TCI, >98.0%), hydrogen peroxide aqueous solution (H_2O_2, Beijing Reagent Co. Ltd., 30 wt %), anhydrous ethanol (C_2H_5OH, Sigma-Aldrich, ≥99.8%), and ammonia aqueous solution (NH_3, Beijing Yili Fine Chemical Co., Ltd., 25−28 wt %) were used as received without further purification. Distilled chloroform was employed as the solvent for porphyrins. Milli-Q water (18 MΩ·cm) was used as solvent for SDBS.

The veritable average peroxide weight percentage of the hydrogen peroxide aqueous solution was assayed to be *ca.* 27.1 ± 2.0% by iodometric titration.[61] For the dosing of our two-end nanoelectronic sensors, H_2O_2 aqueous solutions of *ca.* 0.09, 0.45, and 0.9 wt % were obtained by diluting the original H_2O_2 aqueous solution with Milli-Q water. The vapor-phase concentrations of thus-produced H_2O_2 solutions are *ca.* 0.25, 1.25, and 2.5 ppm, respectively, which are derived according to published data.[60,61,65,68] The temperature of the H_2O_2 vapor was controlled by a water bath of a desired temperature. The assay of the vapor-phase concentrations of C_2H_5OH and NH_3 was carried out according to the methods reported previously.[69,70]

Assembly of Porphyrin Supramolecular Nanoassemblies *via* a SAS. In a typical assembly, 800 μL of a chloroform solution of our porphyrins (2×10^{-4} M) was dropwise added into a 10 mL aqueous solution of SDBS (1.2 mM) under vigorous stirring. Practically, an opaque solution was immediately obtained upon the dropping. After the stirring was performed for *ca.* 20 min for the evaporation of chloroform, a transparent solution could be obtained. To obtain nanoassemblies of an unambiguous morphology,[28,29] the obtained dispersion was left standing for 3 days under ambient conditions, after which their UV−vis spectra were measured and the produced nanostructures were collected by centrifugation (10 000 rpm, 15 min). The samples were then washed fully with Milli-Q water by repeating the centrifugation several times. The as-obtained nanostructures were characterized by means of transmission electron microscopy (TEM), high-resolution transmission electron microscopy (HRTEM), fast Fourier transformation (FFT), scanning electron microscopy (SEM), X-ray diffraction (XRD), and energy-dispersive X-ray spectroscopy (EDX) measurements. On the other hand, the nanostructures could also be obtained by filtration on a Millipore filter (pore size 200 nm). Subsequently, the as-collected nanomaterials were subjected to the above-mentioned characterizations. Similar results were obtained for the samples produced by filtration and centrifugation.

Fabrication of the Single Nanofiber Nanoelectronics and Their Electrical Performances for Vapor-Phase H_2O_2 Sensing. The two-end nanoelectronics using a single TiOTPyP nanofiber as active component were formulated by an organic ribbon mask protocol.[57] Experimentally, the transfer of TiOTPyP nanofibers was achieved by dropping a water dispersion of the nanofibers (*ca.* 120 μL, *ca.* 0.1 mg/mL) onto a Si/SiO_2 (300 nm) substrate. After the evaporation of the water solvent under ambient conditions, the samples were dried in a vacuum oven at room temperature overnight. The as-obtained specimens were then subjected to the construction of two-end electronics. Practically, an individual organic ribbon of an anthracene derivative[58] was picked up by the probe of a Keithley 4200 SCS and a micromanipulator 6150 probe station and was placed across over the TiOTPyP nanofiber. Gold electrodes were then deposited on the samples by thermal evaporation, after which the organic ribbon, which worked as the mask, was peeled up by the probe. The construction of two-end nanosensors could thus be achieved. For the construction of our two-end devices using thin-film geometry, almost similar operations were performed except that a spin-coated film (2000 rpm, 0.5 mL TiOTPyP chloroform solution of 4 mg/mL) of TiOTPyP of *ca.* 100 nm was used as an active component.

The dosing of the two-end nanodevices was performed using a homemade gas delivery system, which consisted of N_2 gas ductwork and N_2/H_2O_2 mixture gas ductwork. Each gas specimen has its own supply. Vapor-phase H_2O_2 was prepared by blowing N_2 gas into a freshly diluted H_2O_2 solution, wherein the H_2O_2 concentration in the vapor phase was controlled by the concentration of the employed H_2O_2 solution.[61] The electrical responses of the nanodevices to the vapor-phase H_2O_2 were recorded with a Keithley 4200-SCS semiconductor parameter analyzer and a micromanipulator 6150 probe station, which were placed in a clean and dark shielded chamber. A fresh H_2O_2 solution, which was diluted to a desired concentration, was used for each dosing run. A sustained bias voltage of 20 V was applied on the nanodevices during the measurements. In the cases of C_2H_5OH and NH_3 gases, almost similar operations were carried out, except that aqueous solutions of C_2H_5OH and NH_3 of desired concentrations were employed.[69,70]

Apparatus and Measurements. A JASCO UV-550 spectrophotometer was used for the measurements of UV−vis spectra. LRTEM and HRTEM images of the assembled supramolecular nanostructures were measured with a FEI Tecnai G2 F20 U-TWIN, wherein the operations were carried out with an accelerating voltage of 80 kV. The SEM measurements were performed using a Hitachi S-4800 system (Japan). XRD measurements were performed on a PANalytical X'Pert PRO instrument with Cu KR radiation. The EDX of the samples was measured with a Horiba EMAX X-act energy-dispersive spectroscope that was attached to the Hitachi S-4800 system.

Conflict of Interest: The authors declare no competing financial interest.

Acknowledgment. This work was supported financially by the National Natural Science Foundation of China (21372225, 20873159, 21321063, and 91027042), the National Key Basic Research Project of China (2011CB932301 and 2013CB834504), and the Chinese Academy of Sciences (XDA09030200 and 1731300500015).

Supporting Information Available: Digital pictures for the assembly of our porphyrins using plain water or an aqueous solution of SDBS surfactant as host solutions. UV−vis spectra and SEM images of the nanoassemblies of H2TPyP and ZnTPyP using plain water as host solution. EDX elemental analyses of the supramolecular nanostructures of our porphyrins. Real-time electrical current changes of our single nanofiber devices to a flow of H_2O_2 vapor at 25 °C. Sensor response of our thin-film devices to a flow of H_2O_2 vapor of *ca.* 2.5 ppm at 25 °C. This material is available free of charge *via* the Internet at http://pubs.acs.org.

REFERENCES AND NOTES

1. Wang, C.; Dong, H.; Hu, W.; Liu, Y.; Zhu, D. Semiconducting π-Conjugated Systems in Field-Effect Transistors: A Material Odyssey of Organic Electronics. *Chem. Rev.* **2012**, *112*, 2208–2267.
2. An, B.-K.; Gierschner, J.; Park, S. Y. π-Conjugated Cyanostilbene Derivatives: A Unique Self-Assembly Motif for Molecular Nanostructures with Enhanced Emission and Transport. *Acc. Chem. Res.* **2012**, *45*, 544–554.
3. Li, R.; Hu, W.; Liu, Y.; Zhu, D. Micro- and Nanocrystals of Organic Semiconductors. *Acc. Chem. Res.* **2010**, *43*, 529–540.
4. Sakakibara, K.; Hill, J. P.; Ariga, K. Thin-Film-Based Nanoarchitectonics for Soft Matter: Controlled Assemblies into Two-Dimensional Worlds. *Small* **2011**, *7*, 1288–1308.
5. Zhang, Z.; Huang, H.; Yang, X.; Zang, L. Tailoring Electronic Properties of Graphene by $\pi-\pi$ Stacking with Aromatic Molecule. *J. Phys. Chem. Lett.* **2011**, *2*, 2897–2905.
6. Yan, Y.; Lin, Y.; Qiao, Y.; Huang, J. Construction and Application of Tunable One-Dimensional Soft Supramolecular Assemblies. *Soft Matter* **2011**, *7*, 6385–6398.
7. Chen, W.; Qi, D.-C.; Huang, H.; Gao, X.; Wee, A. T. S. Organic−Organic Heterojunction Interfaces: Effect of Molecular Orientation. *Adv. Funct. Mater.* **2011**, *21*, 410–424.
8. Chen, W.; Qi, D.; Gao, X.; Wee, A. T. S. Surface Transfer Doping of Semiconductors. *Prog. Surf. Sci.* **2009**, *84*, 279–321.
9. Medforth, C. J.; Wang, Z.; Martin, K. E.; Song, Y.; Jacobsen, J. L.; Shelnutt, J. A. Self-Assembled Porphyrin Nanostructures. *Chem. Commun.* **2009**, 7261–7277.
10. Yoshimoto, S.; Kobayashi, N. Supramolecular Nanostructures of Phthalocyanines and Porphyrins at Surfaces Based on the "Bottom-Up Assembly". *Struct. Bonding* **2010**, *135*, 137–168.
11. Monti, D. Recent Advancements in Chiral Porphyrin Self-Assembly. *Top. Heterocycl. Chem.* **2013**, *33*, 231–292.
12. Ariga, K.; Lee, M. V.; Mori, T.; Yu, X.-Y.; Hill, J. P. Two-Dimensional Nanoarchitectonics Based on Self-Assembly. *Adv. Colloid Interface Sci.* **2010**, *154*, 20–29.
13. Li, M.; Ishihara, S.; Ji, Q.; Akada, M.; Hill, J. P.; Ariga, K. Paradigm Shift from Self-Assembly to Commanded Assembly of Functional Materials: Recent Examples in Porphyrin/Fullerene Supramolecular Systems. *Sci. Technol. Adv. Mater.* **2012**, *13*, 053001.
14. Wang, Z.; Ho, K. J.; Medforth, C. J.; Shelnutt, J. A. Porphyrin Nanofiber Bundles from Phase-Transfer Ionic Self-Assembly and Their Photocatalytic Self-Metallization. *Adv. Mater.* **2006**, *18*, 2557–2560.
15. Ozawa, H.; Tanaka, H.; Kawao, M.; Uno, S.; Nakazato, K. Preparation of Organic Nanoscrews from Simple Porphyrin Derivatives. *Chem. Commun.* **2009**, 7411–7413.
16. Huang, C.; Li, Y.; Song, Y.; Li, Y.; Liu, H.; Zhu, D. Ordered Nanosphere Alignment of Porphyrin for the Improvement of Nonlinear Optical Properties. *Adv. Mater.* **2010**, *22*, 3532–3536.
17. Wang, Z.; Medforth, C. J.; Shelnutt, J. A. Self-Metallization of Photocatalytic Porphyrin Nanotubes. *J. Am. Chem. Soc.* **2004**, *126*, 16720–16721.
18. Wang, L.; Liu, H.; Hao, J. Stable Porphyrin Vesicles Formed in Non-aqueous Media and Dried To Produce Hollow Shells. *Chem. Commun.* **2009**, 1353–1355.
19. Hu, J.-S.; Guo, Y.-G.; Liang, H.-P.; Wan, L.-J.; Jiang, L. Three-Dimensional Self-Organization of Supramolecular Self-Assembled Porphyrin Hollow Hexagonal Nanoprisms. *J. Am. Chem. Soc.* **2005**, *127*, 17090–17095.
20. Huang, C.; Wen, L.; Liu, H.; Li, Y.; Liu, X.; Yuan, M.; Zhai, J.; Jiang, L.; Zhu, D. Controllable Growth of 0D to Multidimensional Nanostructures of a Novel Porphyrin Molecule. *Adv. Mater.* **2009**, *21*, 1721–1725.
21. Li, Y.; Li, X.; Li, Y.; Liu, H.; Wang, S.; Gan, H.; Li, J.; Wang, N.; He, X.; Zhu, D. Controlled Self-Assembly Behavior of an Amphiphilic Bisporphyrin−Bipyridinium−Palladium Complex: From Multibilayer Vesicles to Hollow Capsules. *Angew. Chem., Int. Ed.* **2006**, *45*, 3639–3643.
22. Gao, Y.; Zhang, X.; Ma, C.; Li, X.; Jiang, J. Morphology-Controlled Self-Assembled Nanostructures of 5,15-Di[4-(5-acetylsulfanylpentyloxy)phenyl]porphyrin Derivatives. Effect of Metal−Ligand Coordination Bonding on Tuning the Intermolecular Interaction. *J. Am. Chem. Soc.* **2008**, *130*, 17044–17052.
23. Lu, G.; Chen, Y.; Zhang, Y.; Bao, M.; Bian, Y.; Li, X.; Jiang, J. Morphology Controlled Self-Assembled Nanostructures of Sandwich Mixed (Phthalocyaninato)(Porphyrinato) Europium Triple-Deckers. Effect of Hydrogen Bonding on Tuning the Intermolecular Interaction. *J. Am. Chem. Soc.* **2008**, *130*, 11623–11630.
24. Wang, Z.; Li, Z.; Medforth, C. J.; Shelnutt, J. A. Self-Assembly and Self-Metallization of Porphyrin Nanosheets. *J. Am. Chem. Soc.* **2007**, *129*, 2440–2441.
25. Hasobe, T.; Sandanayaka, A. S. D.; Wada, T.; Araki, Y. Fullerene-Encapsulated Porphyrin Hexagonal Nanorods. An Anisotropic Donor−Acceptor Composite for Efficient Photoinduced Electron Transfer and Light Energy Conversion. *Chem. Commun.* **2008**, 3372–3374.
26. Ji, H.-X.; Hu, J.-S.; Wan, L.-J. ZnOEP Based Phototransistor: Signal Amplification and Light-Controlled Switch. *Chem. Commun.* **2008**, 2653–2655.
27. Schwab, A. D.; Smith, D. E.; Bond-Watts, B.; Johnston, D. E.; Hone, J.; Johnson, A. T.; de Paula, J. C.; Smith, W. F. Photoconductivity of Self-Assembled Porphyrin Nanorods. *Nano Lett.* **2004**, *4*, 1261–1265.

28. Qiu, Y.; Chen, P.; Liu, M. Evolution of Various Porphyrin Nanostructures *via* an Oil/Aqueous Medium: Controlled Self-Assembly, Further Organization, and Supramolecular Chirality. *J. Am. Chem. Soc.* **2010**, *132*, 9644–9652.
29. Guo, P.; Chen, P.; Liu, M. Porphyrin Assemblies *via* a Surfactant-Assisted Method: From Nanospheres to Nanofibers with Tunable Length. *Langmuir* **2012**, *28*, 15482–15490.
30. Guo, P.; Chen, P.; Liu, M. One-Dimensional Porphyrin Nanoassemblies Assisted *via* Graphene Oxide: Sheetlike Functional Surfactant and Enhanced Photocatalytic Behaviors. *ACS Appl. Mater. Interfaces* **2013**, *5*, 5336–5345.
31. Guo, P.; Chen, P.; Ma, W.; Liu, M. Morphology-Dependent Supramolecular Photocatalytic Performance of Porphyrin Nanoassemblies: From Molecule to Artificial Supramolecular Nanoantenna. *J. Mater. Chem.* **2012**, *22*, 20243–20249.
32. Labuta, J.; Ishihara, S.; Šikorský, T.; Futera, Z.; Shundo, A.; Hanyková, L.; Burda, J. V.; Ariga, K.; Hill, J. P. NMR Spectroscopic Detection of Chirality and Enantiopurity in Referenced Systems without Formation of Diastereomers. *Nat. Commun.* **2013**, *4*, 2188.
33. Shundo, A.; Ishihara, S.; Labuta, J.; Onuma, Y.; Sakai, H.; Abe, M.; Ariga, K.; Hill, J. P. Colorimetric Visualization of Acid−Base Equilibria in Non-polar Solvent. *Chem. Commun.* **2013**, *49*, 6870–6872.
34. Ishihara, S.; Iyi, N.; Labuta, J.; Deguchi, K.; Ohki, S.; Tansho, M.; Shimizu, T.; Yamauchi, Y.; Sahoo, P.; Naito, M.; Abe, H.; Hill, J. P.; Ariga, K. Naked-Eye Discrimination of Methanol from Ethanol Using Composite Film of Oxoporphyrinogen and Layered Double Hydroxide. *ACS Appl. Mater. Interfaces* **2013**, *5*, 5927–5930.
35. Kasha, M.; Rawls, H. R.; Ashraf El-Bayoumi, M. The Exciton Model in Molecular Spectroscopy. *Pure Appl. Chem.* **1965**, *11*, 371–392.
36. Zhang, Y.; Chen, P.; Liu, M. A General Method for Constructing Optically Active Supramolecular Assemblies from Intrinsically Achiral Water-Insoluble Free-Base Porphyrins. *Chem.—Eur. J.* **2008**, *14*, 1793–1803.
37. McRae, E. G.; Kasha, M. Enhancement of Phosphorescence Ability upon Aggregation of Dye Molecules. *J. Chem. Phys.* **1958**, *28*, 721–722.
38. Zhang, Y.; Chen, P.; Ma, Y.; He, S.; Liu, M. Acidification and Assembly of Porphyrin at an Interface: Counterion Matching, Selectivity, and Supramolecular Chirality. *ACS Appl. Mater. Interfaces* **2009**, *1*, 2036–2043.
39. Qian, D.-J.; Nakamura, C.; Miyake, J. Multiporphyrin Array from Interfacial Metal-Mediated Assembly and Its Langmuir−Blodgett Films. *Langmuir* **2000**, *16*, 9615–9619.
40. Maiti, N. C.; Mazumdar, S.; Periasamy, N. J- and H-Aggregates of Porphyrin−Surfactant Complexes: Time-Resolved Fluorescence and Other Spectroscopic Studies. *J. Phys. Chem. B* **1998**, *102*, 1528–1538.
41. Gandini, S. C. M.; Yushmanov, V. E.; Borissevitch, I. E.; Tabak, M. Interaction of the Tetra(4-sulfonatophenyl)porphyrin with Ionic Surfactants: Aggregation and Location in Micelles. *Langmuir* **1999**, *15*, 6233–6243.
42. Mishra, P. P.; Bhatnagar, J.; Datta, A. The Interplay of Hydrophobic and Electrostatic Effects in the Surfactant-Induced Aggregation/Deaggregation of Chlorin p6. *J. Phys. Chem. B* **2005**, *109*, 24225–24230.
43. Steinbeck, C. A.; Hedin, N.; Chmelka, B. F. Interactions of Charged Porphyrins with Nonionic Triblock Copolymer Hosts in Aqueous Solutions. *Langmuir* **2004**, *20*, 10399–10412.
44. Fleischer, E. B.; Miller, C. K.; Webb, L. E. Crystal and Molecular Structures of Some Metal Tetraphenylporphines. *J. Am. Chem. Soc.* **1964**, *86*, 2342–2347.
45. Yu, W.; Li, Z.; Wang, T.; Liu, M. Aggregation and Supramolecular Chirality of Achiral Amphiphilic Metalloporphyrins. *J. Colloid Interface Sci.* **2008**, *326*, 460–464.
46. Yao, P.; Qiu, Y.; Chen, P.; Ma, Y.; He, S.; Zheng, J.-Y.; Liu, M. Interfacial Molecular Assemblies of Metalloporphyrins with Two Trans or One Axial Ligands. *ChemPhysChem* **2010**, *11*, 722–729.
47. Li, X.; Zheng, Z.; Han, M.; Chen, Z.; Zou, G. Tuning J-Aggregates of Tetra(*p*-hydroxyphenyl)porphyrin by the Headgroups of Ionic Surfactants in Acidic Nonionic Micellar Solution. *J. Phys. Chem. B* **2007**, *111*, 4342–4348.
48. Kadish, K. M.; Maiya, B. G.; Araullo-McAdams, C. Spectroscopic Characterization of *meso*-Tetrakis(l-methylpyridinium-4-yl)porphyrins, $[(TMpyP)H_2]^{4+}$ and $[(TMpyP)M]^{4+}$, in Aqueous Micellar Media, Where M = VO^{2+}, Cu(II), and Zn(II). *J. Phys. Chem.* **1991**, *95*, 427–431.
49. Hunter, C. A.; Sanders, J. K. M. The Nature of $\pi-\pi$ Interactions. *J. Am. Chem. Soc.* **1990**, *112*, 5525–5534.
50. Ruggles, J. L.; Foran, G. J.; Tanida, H.; Nagatani, H.; Jimura, Y.; Watanabe, I.; Gentle, I. R. Interfacial Behavior of Tetrapyridylporphyrin Monolayer Arrays. *Langmuir* **2006**, *22*, 681–686.
51. Würthner, F.; Kaiser, T. E.; Saha-Möller, C. R. J-Aggregates: From Serendipitous Discovery to Supramolecular Engineering of Functional Dye Materials. *Angew. Chem., Int. Ed.* **2011**, *50*, 3376–3416.
52. Kong, J.; Franklin, N. R.; Zhou, C.; Chapline, M. G.; Peng, S.; Cho, K.; Dai, H. Nanotube Molecular Wires as Chemical Sensors. *Science* **2000**, *287*, 622–625.
53. Tang, Q.; Li, L.; Song, Y.; Liu, Y.; Li, H.; Xu, W.; Liu, Y.; Hu, W.; Zhu, D. Photoswitches and Phototransistors from Organic Single-Crystalline Sub-micro/nanometer Ribbons. *Adv. Mater.* **2007**, *19*, 2624–2628.
54. Patolsky, F.; Lieber, C. M. Nanowire Nanosensors. *Mater. Today* **2005**, *8*, 20–28.
55. Zhao, G.; Dong, H.; Jiang, L.; Zhao, H.; Qin, X.; Hu, W. Single Crystal Field-Effect Transistors Containing a Pentacene Analogue and Their Application in Ethanol Vapor Detection. *Appl. Phys. Lett.* **2012**, *101*, 103302−1–103302−3.
56. Shaymurat, T.; Tang, Q.; Tong, Y.; Dong, L.; Liu, Y. Gas Dielectric Transistor of CuPc Single Crystalline Nanowire for SO_2 Detection Down to Sub-ppm Levels at Room Temperature. *Adv. Mater.* **2013**, *25*, 2269–2273.
57. Jiang, L.; Gao, J.; Wang, E.; Li, H.; Wang, Z.; Hu, W.; Jiang, L. Organic Single-Crystalline Ribbons of a Rigid "H"-Type Anthracene Derivative and High-Performance, Short-Channel Field-Effect Transistors of Individual Micro/Nanometer-Sized Ribbons Fabricated by an "Organic Ribbon Mask" Technique. *Adv. Mater.* **2008**, *20*, 2735–2740.
58. Jiang, L.; Fu, Y.; Li, H.; Hu, W. Single-Crystalline, Size, and Orientation Controllable Nanowires and Ultralong Microwires of Organic Semiconductor with Strong Photoswitching Property. *J. Am. Chem. Soc.* **2008**, *130*, 3937–3941.
59. Bohrer, F. I.; Sharoni, A.; Colesniuc, C.; Park, J.; Schuller, I. K.; Kummel, A. C.; Trogler, W. C. Gas Sensing Mechanism in Chemiresistive Cobalt and Metal-Free Phthalocyanine Thin Films. *J. Am. Chem. Soc.* **2007**, *129*, 5640–5646.
60. Manatt, S. L.; Manatt, M. R. R. On the Analyses of Mixture Vapor Pressure Data: The Hydrogen Peroxide/Water System and Its Excess Thermodynamic Functions. *Chem.—Eur. J.* **2004**, *10*, 6540–6557.
61. Zheng, J. Y.; Yan, Y.; Wang, X.; Shi, W.; Ma, H.; Zhao, Y. S.; Yao, J. Hydrogen Peroxide Vapor Sensing with Organic Core/Sheath Nanowire Optical Waveguides. *Adv. Mater.* **2012**, *24*, OP194–OP197.
62. Germain, M. E.; Knapp, M. J. Optical Explosives Detection: From Color Changes to Fluorescence Turn-On. *Chem. Soc. Rev.* **2009**, *38*, 2543–2555.
63. Schulte-Ladbeck, R.; Vogel, M.; Karst, U. Recent Methods for the Determination of Peroxide-Based Explosives. *Anal. Bioanal. Chem.* **2006**, *386*, 559–565.
64. Cui, Q. H.; Zhao, Y. S.; Yao, J. Tailoring the Structures and Compositions of One-Dimensional Organic Nanomaterials towards Chemical Sensing Applications. *Chem. Sci.* **2013**, *5*, 52–57.
65. Bohrer, F. I.; Colesniuc, C. N.; Park, J.; Schuller, I. K.; Kummel, A. C.; Trogler, W. C. Selective Detection of Vapor Phase Hydrogen Peroxide with Phthalocyanine Chemiresistors. *J. Am. Chem. Soc.* **2008**, *130*, 3712–3713.
66. Royer, J. E.; Kappe, E. D.; Zhang, C.; Martin, D. T.; Trogler, W. C.; Kummel, A. C. Organic Thin-Film Transistors for Selective Hydrogen Peroxide and Organic Peroxide Vapor Detection. *J. Phys. Chem. C* **2012**, *116*, 24566–24572.

67. Riley, C. K.; Muller, E. A.; Feldman, B. E.; Cross, C. M.; Van Aken, K. L.; Johnston, D. E.; Lu, Y.; Johnson, A. T.; de Paula, J. C.; Smith, W. F. Effects of O_2, Xe, and Gating on the Photoconductivity and Persistent Photoconductivity of Porphyrin Nanorods. *J. Phys. Chem. C* **2010**, *114*, 19227–19233.
68. Xu, M.; Bunes, B. R.; Zang, L. Paper-Based Vapor Detection of Hydrogen Peroxide: Colorimetric Sensing with Tunable Interface. *ACS Appl. Mater. Interfaces* **2011**, *3*, 642–647.
69. Perman, E. P. Vapour Pressure of Aqueous Ammonia Solution. Part II. *J. Chem. Soc., Trans.* **1903**, *83*, 1168–1184.
70. Errington, J. R.; Boulougouris, G. C.; Economou, I. G.; Panagiotopoulos, A. Z.; Theodorou, D. N. Molecular Simulation of Phase Equilibria for Water–Methane and Water–Ethane Mixtures. *J. Phys. Chem. B* **1998**, *102*, 8865–8873.